PERGAMON

International Journal of Heat and Mass Transfer 41 (1998) 3191–3201

International Journal of HEAT and MASS TRANSFER

Observation of boiling structures in high heat-flux boiling

Shigefumi Nishio[a,*], Tetsushi Gotoh[a], Niroh Nagai[b]

[a] *Institute of Industrial Science, University of Tokyo, 7-22-1 Roppongi, Minato-ku, Tokyo 106, Japan*
[b] *Department of Mechanical Engineering, Fukui University, 3-9-1 Bunkyo, Fukui City, Fukui 910, Japan*

Received 27 October 1997; in final form 21 January 1998

Abstract

This study is an attempt to attain a good understanding of boiling structures such as liquid–solid contact patterns and bubble structures near the boiling surface. This was accomplished by observing both the dynamic behavior of liquid–solid contact from below the surface and the sectional views of bubbles in a quasi-two-dimensional boiling space. Results of the observation indicate that the boiling structures at heat fluxes near the CHF point are different from the physical image given by the so-called macrolayer model. Based on this fact, we propose a new concept of the contact-line-length density describing the contribution of evaporating thin liquid layers to high-heat-flux boiling heat transfer.

Nomenclature

b half value of averaged distance between centers of dry areas
C heat transfer coefficient of vaporization
D equivalent diameter of dry area
D_m averaged equivalent diameter of dry area
$D_{p,max}$ maximum value of equivalent diameter of primary dry area
h height of liquid–vapor interface
h_{lv} latent heat of vaporization
H height of glass plates
k thermal conductivity of liquid
M molecular weight
n_D number of dry areas in each diameter class
N_D number density of dry areas
q heat flux
q_{cl} heat flux at evaporating contact line
q_{CHF} critical heat flux
$q_{CHF,Z}$ critical heat flux value estimated by Zuber equation
$Q_{L,90}$ heat transfer rate per unit contact line length
R_0 universal gas constant
t time
T_{sat} saturation temperature
T_w temperature of boiling surface
W width of boiling surface.

Greek symbols
α evaporation coefficient
Γ_w time- and space-averaged fraction of liquid–solid contact
$\delta_{l,max}$ averaged height of vapor domes
$\delta_{l,mix}$ liquid subfilm thickness under coalescent bubbles
ΔT_{CHF} surface superheat at CHF point
ΔT_{ws} surface superheat
θ contact angle
λ_{cp} Laplace length
λ_n solutions of equation (3)
ρ_v density of vapor
Φ contact-line-length density
Φ_{max} maximum value of contact-line-length density.

1. Introduction

The evaporation and boiling phenomena are very important as an elementary process in the energy equipment such as power plants producing steam and also in the thermal management technology for materials processing and electronic operation systems. While these applications have promoted understanding of the heat transfer and structural aspects of the boiling phenomena, the recent advent of microsystems such as bubble jet printers and micro actuators asks for a better under-

* Corresponding author.

0017–9310/98 $19.00
PII: S0017–9310(98)00062–3

standing of the boiling phenomena from the structural viewpoints in particular.

In general, the structure formation in the phase change of liquid can be regarded as the result of the series of the following elementary phenomena which relate fundamentally to the molecular dynamics in phase change, the dynamics of moving contact lines, and the interfacial stability; (1) formation of supersaturated liquid phase, (2) nucleation of new phase or activation of preexisting nuclei, (3) growth of new phase, and (4) formation of interface morphology. For example, Asai [1] has presented a boiling model for bubble jet printers in which a coalescent bubble with smooth interface grows as the result of the series of formation of extremely superheated liquid-phase, the spontaneous bubble nucleation, and simultaneous growth of primary bubbles.

As for the steady-state nucleate boiling at high heat fluxes, Gaertner [2] reported the following time-averaged structure based on still photographs and high-speed motion pictures of boiling. The first layer is the liquid layer including numerous columnar stems of vapor attached to the boiling surface. This layer has been called the macrolayer. The second layer includes large mushroom bubbles formed by coalescence of the vapor stems. Gigantic vapor slugs exist in the third layer and they result from coalescence of the mushroom bubbles rising up from the second layer. In this paper, this model is called the three-layered boiling-structure model.

The three-layered model is very important because it has given the typical image of high heat-flux boiling including transition boiling. For example, based on this model, Haramura and Katto [3] proposed the 'macrolayer dryout model' and also Dhir and Liaw [4] proposed the 'unified model' for the critical heat flux (CHF) in natural convection boiling. The existence of a liquid film under the mushroom bubble was observed certainly by Katto and Yokoya [5]. In their experiment, the behavior of the liquid film under a mushroom bubble was observed by setting an optical equipment very close to the surface and they reported that CHF in natural convection boiling related closely to the dryout of the liquid film (macrolayer) and the periodic departure of mushroom bubbles. However, the most important problem in the three-layered model is the structure of the first layer. The CHF models mentioned above assume stationary vapor stems of small diameters attached to the boiling surface, but this situation is very different from the results of observation reported by Nagai and Nishio [6] and Oka et al. [7]. A new attempt should be thus made to observe the boiling structures on/near the surface such as liquid–solid contact patterns and bubble structures.

One of the difficulties in the observation of real boiling structures is that the three-dimensional and dynamic motion of bubbles obstructs our view of the real boiling structure on/near the boiling surface. In our study, thus, the following attempts were made to observe directly the boiling structures. One is an attempt to observe directly the dynamic behavior of liquid–solid contact from below the boiling surface by using a horizontal plate of single crystal sapphire as the boiling surface. The other is an attempt to observe the sectional views of bubble structures by using a quasi-two-dimensional boiling system. The physical image of boiling structures obtained in these attempts is much different from the three-layered model.

2. Observation of liquid–solid contact pattern and concept of contact-line-length density

2.1. Total reflection technique

Figure 1 illustrates a schematic diagram of the experimental apparatus to observe directly the dynamic behavior of liquid–solid contact in natural-convection boiling.

A xenon light beam is introduced to a transparent boiling surface from below the surface through a silicone oil bath. The transparent boiling surface should be made of highly conductive material because the thermal conductivity of the surface material has strong effects on the boiling curve (for example, Nishio [8]). In this experiment, a plate of single crystal sapphire was selected as the boiling surface because its thermal conductivity is almost the same as stainless steel. The plate thickness was 5 mm.

When the incidence angle of the light beam is set adequately, total reflection occurs at the surface if the surface is dry and it does not occur if the surface is wetted by the liquid. So, clear pictures of the dynamic behavior

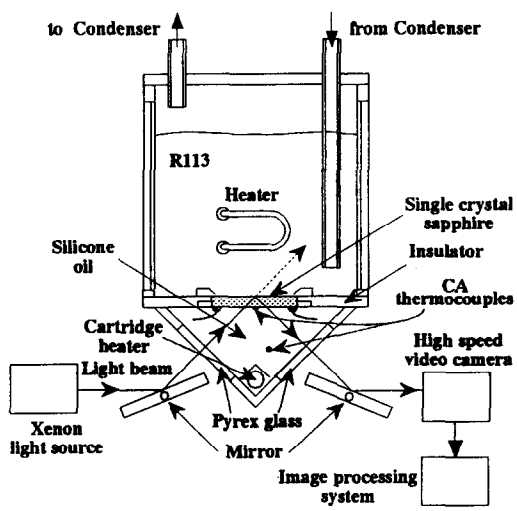

Fig. 1. Schematic diagram of experimental apparatus to observe dynamic behavior of liquid–solid contact.

of liquid–solid contact can be obtained by recording them using a high-speed video system (Nagai and Nishio [9]).

The test liquid was R-113 at atmospheric pressure. The temperature of the liquid was maintained at the saturation temperature by an electric heater. The boiling surface was heated by supplying a DC electric current to an electro-conductive transparent film coated on the back side of the sapphire plate. In the nucleate and film boiling regions, the temperature of the silicone oil bath was controlled equal to that of the thin film to reduce heat loss from the film. For these regions, the observation was conducted under steady-state conditions by increasing or decreasing the DC current step by step. The surface temperature was measured with thermocouples attached to the surface and also with the electric resistance of the thin film. The heat flux was given by Joule heating of the thin film. As for the transition boiling region, the observation was conducted during transient periods from nucleate to film boiling or from film to nucleate boiling. In this case, the boiling curve was calculated by using an inverse heat-conduction technique based on the surface temperature histories.

2.2. Liquid–solid contact patterns

Figure 2 shows a typical set of pictures of liquid–solid contact patterns from the non-boiling to film boiling regions recorded by the high-speed video system. The white areas in each picture correspond to dry areas and the black areas to wetted areas. Using such video pictures and an image processing technique, the distribution of the diameter of dry areas and the fraction of liquid–solid contact were calculated. The results were plotted in Figs 3 and 4. The abscissa of Fig. 3 is the equivalent diameter, D, which is the diameter of the circle of the same area as the actual dry area. Dividing the equivalent diameter to classes of $\Delta D = 0.1$ mm, the number of dry areas in each diameter class, n_D, was counted during 400 ms for a surface area of 7.6×7.6 mm. This number n_D is the ordinate in Fig. 3. The fraction of liquid–solid contact averaged for 400 ms, $\Gamma_{v,t}$, was plotted to the normalized surface superheat $\Delta T_{ws}/\Delta T_{CHF}$ in Fig. 4 together with existing data (Ragheb and Chen [10], Lee et al. [11], Dhuga and Winterton [12], Neti et al. [13], and Shoji and Kuroki [14]).

Figure 2(a) corresponds to the non-boiling region because any dry area cannot be observed. Figure 2(b) shows the situation at a surface superheat just above the incipience of nucleate boiling, and a few round dry areas appear which can be regarded as the bases of isolated bubbles. In this paper, the dry areas of such a round shape are called the primary dry areas.

In Figs 2(c) and (d), dry areas remain almost round but the number of dry areas increases with the increases of ΔT_{ws}. As shown in Fig. 3, the distribution of dry area size is different from that of droplet size in dropwise condensation which has a fractal structure (Tanasawa [15]). For example, at $\Delta T_{ws} = 38$ and 44 K corresponding to Figs 2(c) and (d), n_D is almost independent of D for about $D < 0.9$ mm and it decreases rapidly for $D > 0.9$ mm. In the case of Fig. 2(d) corresponding to high heat-flux nucleate boiling, we can observe also some dry areas whose shape becomes not round but slightly distorted due to coalescence of neighboring primary dry areas. The dry areas with such distorted shapes are called the secondary dry areas. It is considered that dry areas in the constant n_D region in Fig. 3 correspond to the primary dry areas and those in the rapidly decreasing n_D region to the secondary dry areas. Anyway, in Figs 2(b)–(d), the wetted area is a continuous plane. The liquid–solid contact of this pattern is called the liquid–solid contact of the continuous plane pattern. As shown in Fig. 4, the present data of the fraction of liquid–solid contact is smaller than one even at high-heat-flux nucleate boiling corresponding to $\Delta T_{ws}/\Delta T_{CHF} = 0.94$ ($\Delta T_{ws} = 44$ K).

Figure 2(e) shows the situation at the CHF point. As shown in Fig. 3, compared with the case at $\Delta T_{ws} = 44$ K, the constant n_D region is shifted to smaller diameters and the numbers, n_D, in a large diameter region are increased. As a result, the fraction of liquid–solid contact is decreased below 60%. In this situation, dry areas become closely packed and the wetted area exists only like a network of wriggling continuous canals of liquid. In this paper, this situation of contact is called the liquid–solid contact of the network pattern. The liquid–solid contact of the network pattern was observed also by Oka et al. [7], but it is much different from the three-layered boiling-structure model in which isolated vapor stems of small diameters are attached to the boiling surface. The result noted above indicates that the primary and second dry areas contribute to decrease the fraction of liquid–solid contact.

In the case of Fig. 2(f) corresponding to high heat-flux transition boiling, there are extremely distorted and large dry areas which seem to result from coalescence of neighboring secondary dry areas. In this paper, such dry areas are called the tertiary dry areas. In the tertiary dry areas, we can find also wetted areas which are isolated from the liquid network and include the primary or secondary dry areas. In this situation, dry areas are divided into the outer dry areas such as the tertiary dry areas and the inner dry areas located in the wetted areas isolated from the liquid network.

In Figs 3(g)–(i), the outer dry area occupies the main portion of the boiling surface and wetted areas exist only as isolated areas. In this paper, this situation is called the liquid–solid contact of the isolated pattern. Figure 2(j) shows the situation of film boiling at a low heat flux and any wetted area cannot be observed.

2.3. Contact-line-length density

As already mentioned, the fraction of liquid–solid contact is decreased not only by the tertiary or outer dry

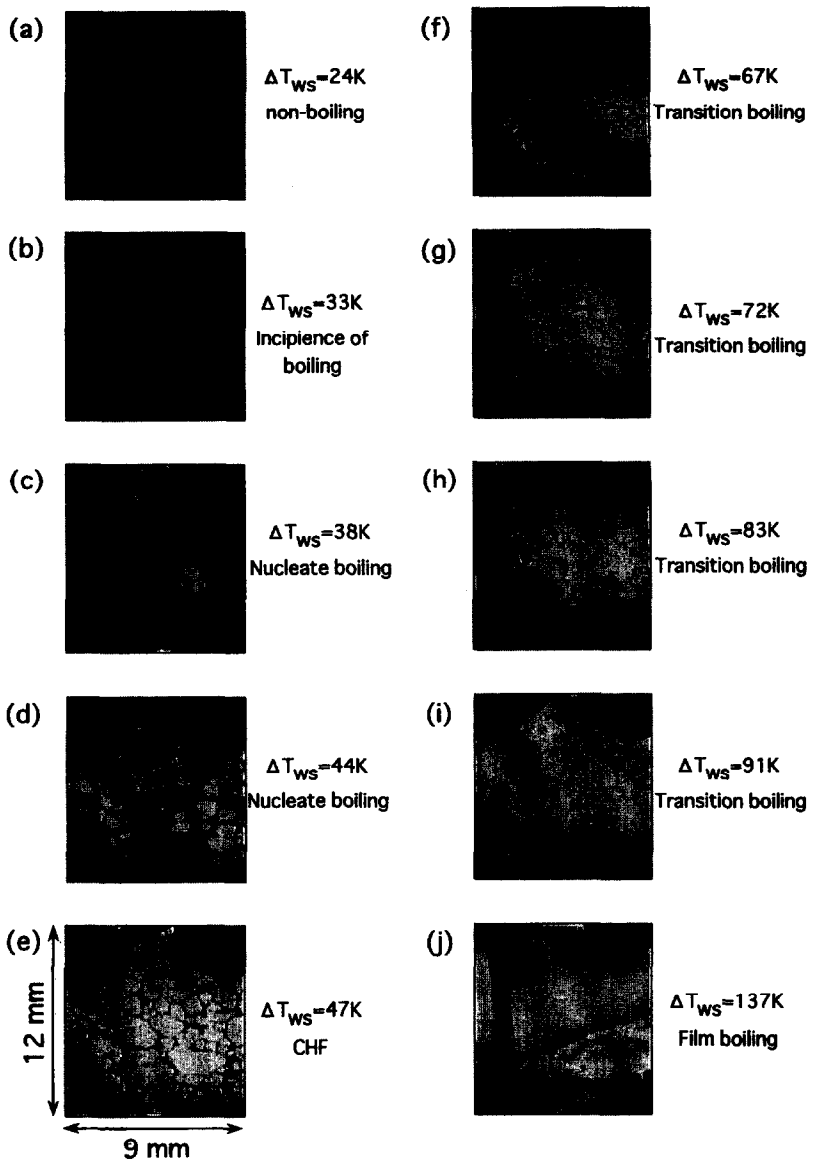

Fig. 2. Dependence of liquid–solid contact pattern on surface temperature.

areas but also by the primary and secondary dry areas. On the other hand, following the literature (for example, Carey [16], and Dhir and Liaw [4]), very intensive evaporation occurs near the contact line. In addition, Graham and Hendricks [17] reported analytical results that the microlayer evaporation contributes largely to the heat flux in high heat-flux nucleate boiling. So, to take account of the contribution of the three types of dry areas to boiling heat transfer, we should focus on the evaporation near the contact line surrounding each dry area. Then, to do this, we define the contact-line-length density, Φ, as the total length of contact lines existing on unit area of the boiling surface. The contact-line-length density is a concept different from the fraction of liquid–solid contact. As an example, we consider the following two cases with the same fraction of liquid–solid contact; one is the case when there is only one large dry area, and the other is the case when there are many tiny dry spots. Comparing these two cases, the contact-line-length density in the former case is much smaller than that in the latter case.

Figure 5 shows experimental data of the fluctuation of the instantaneous contact-line-length density, $\Phi[t]$, calculated from the video pictures by using the image pro-

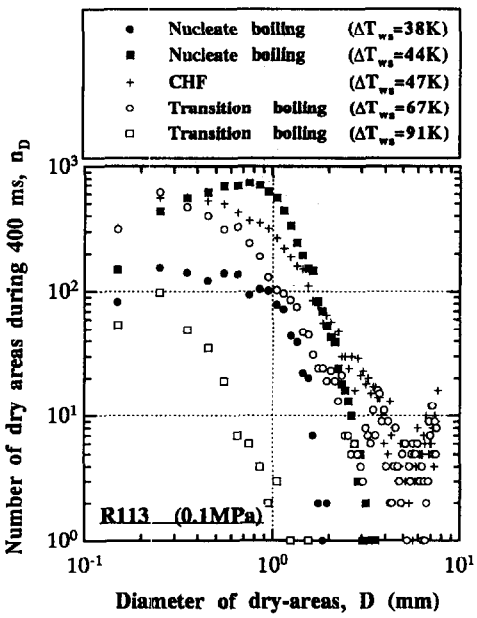

Fig. 3. Distribution of dry-area size.

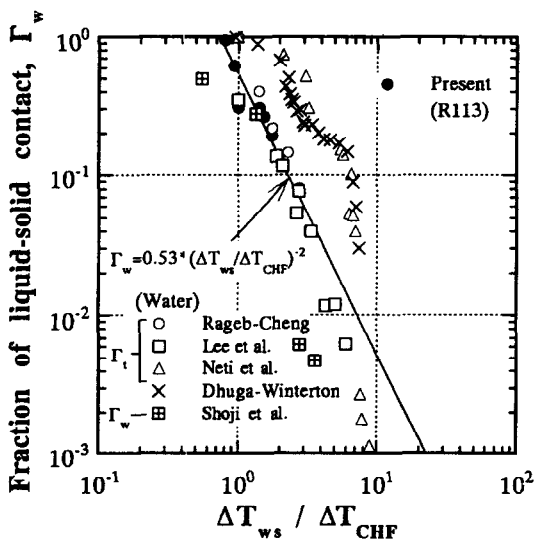

Fig. 4. Experimental data of fraction of liquid–solid contact.

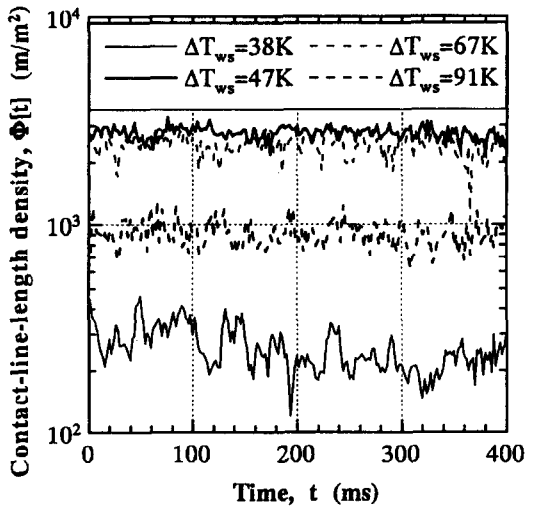

Fig. 5. Fluctuation of contact-line-length density.

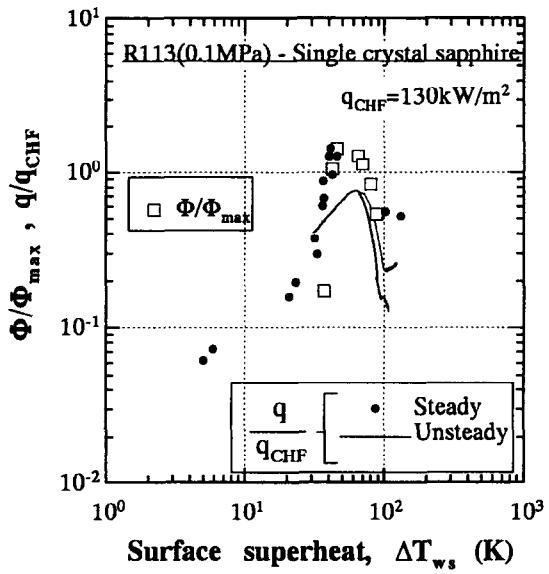

Fig. 6. Normalized contact-line-length density and boiling curve.

cessing technique. Here, it should be noted that, as shown in Fig. 5, the instantaneous contact-line-length density has fluctuations because individual dry area grows, shrinks and also migrates on the boiling surface. The contact-line-length density based on unit area of 1×1 m is as high as the order of magnitude of kilometers at $\Delta T_{ws} = 47$ K corresponding to the CHF point. The time-averaged value of the contact-line-length density normalized by its maximum value, Φ/Φ_{max}, is plotted in Fig. 6 together with the normalized boiling curve measured in this experiment, q/q_{CHF}. As seen from the figure, the dependence of Φ/Φ_{max} on the surface superheat is very similar to that of the normalized boiling curve. This result indicates that the contact-line-length density must be one of the very important quantities representing the boiling structures and also it is a more direct measure compared with the fraction of liquid–solid contact.

The reason why the contact-line-length density has a peak value as shown in Fig. 6 can be explained as follows. The primary dry areas shown in Figs 2(b)–(d) experience the process of generation, growth, shrinkage and disappearance. So, each primary dry area reaches a

maximum diameter during its lifetime, and experimental data of the maximum diameter, $D_{p,max}$, are plotted against the surface superheat in Fig. 7. It is found that the maximum diameter of primary dry areas gradually increases as the surface superheat increases. The increase in surface superheat also brings about rapid increase in nucleation site density. As a result, the contact-line-length density increases with increase of the surface superheat as long as the coalescence of dry areas rarely occurs. On the other hand, the increase of nucleation site density and $D_{p,max}$ induces the coalescence of the primary dry areas resulting in formation of the secondary or tertiary dry areas. Appearance of these secondary or tertiary dry areas decreases the number density of dry areas of smaller diameters as shown in Fig. 3. As a result, the contact-line-length density reaches a maximum value and comes to decrease as the surface superheat increases.

Next, to examine the relation of the value of the contact-line-length density to the boiling curve, we tried to predict the boiling curve by using the experimental data of the contact-line-length density. Following Dhir and Liaw [4], the heat transfer rate per unit contact line length, $Q_{L,90}$ (W m^{-1}), can be calculated by the following equation if the contact angle is assumed $\theta = 90°$ (see Fig. 8).

$$Q_{L,90} = 2C\Delta T_{ws} \sum_{n=1}^{\infty} \frac{\sin 2\lambda_n b(1-\exp[-\lambda_n h])}{(2\lambda_n b+\sin 2\lambda_n b)\lambda_n} \tag{1}$$

$$C = \alpha\rho_v h_{lv}^2 \sqrt{\frac{M}{2\pi R_0 T_{sat}^3}} \tag{2}$$

$$\lambda_n b \tan \lambda_n b = \frac{Cb}{k} \tag{3}$$

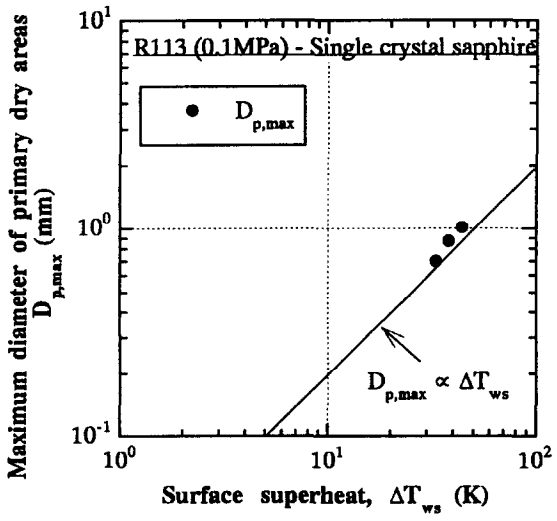

Fig. 7. Maximum diameter of primary dry area.

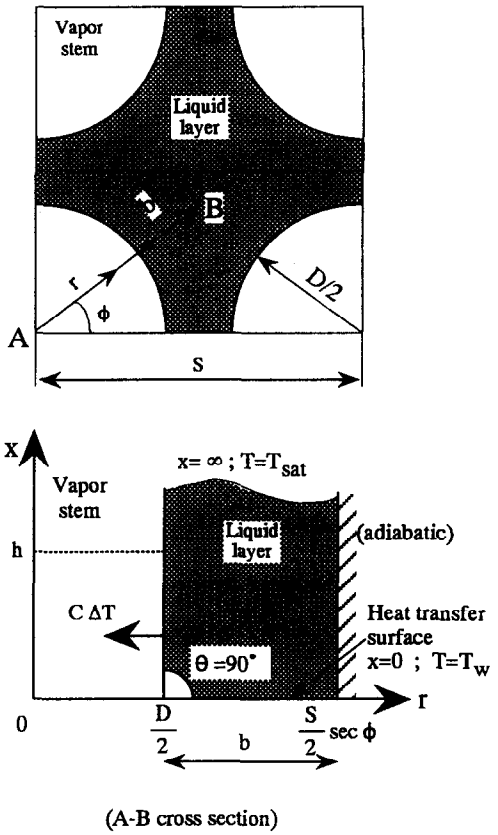

Fig. 8. Boiling-structure model by Dhir and Liaw.

$$b = \frac{1}{2}\sqrt{\frac{1}{\sqrt{N_D}}} - D_m \tag{4}$$

where, α: evaporation coefficient, ρ_v: density of vapor, h_{lv}: latent heat of vaporization, M: molecular weight, R_0: universal gas constant, T_{sat}: saturation temperature, k: thermal conductivity of liquid, N_D: number density of dry areas, h: height of liquid–vapor interface, and D_m: averaged equivalent diameter of dry areas. The values of N_D and D_m can be calculated from the data shown in Fig. 3. Coupling the above equations with the experimental data of Φ, the heat flux at evaporating contact lines, $q_{cl}[\Delta T]$, can be calculated by the following simple equation.

$$q_{cl}[\Delta T_{ws}] = F[\theta]Q_{L,90}[\Delta T_{ws}]\Phi[\Delta T_{ws}]. \tag{5}$$

In this equation, $F[\theta]$ is a function representing the effect of the contact angle on evaporation near the contact line. In this paper, this function is estimated from the graphical result presented by Dhir and Liaw [4].

Based on our preliminary calculations changing h = 1–10 mm, it was concluded that $q_{cl}[\Delta T_{ws}]$ does not depend strongly on the value of h. So, the boiling curves calculated from equations (5) for h = 1 mm and θ = 10, 30

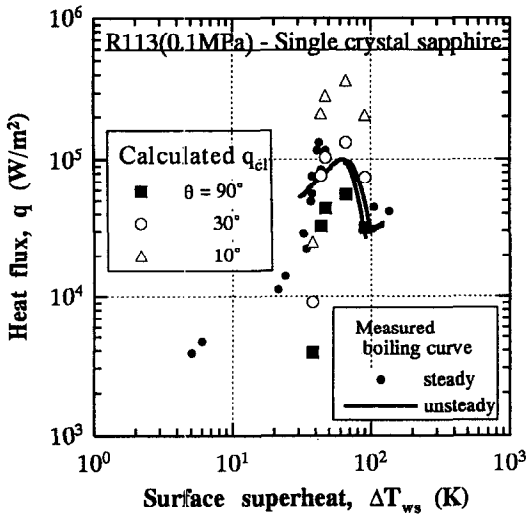

Fig. 9. Comparison between predicted and measured boiling curves.

and 90° are shown in Fig. 9 together with the boiling curves measured in this experiment. As shown in this figure, the boiling curve calculated for $\theta = 30°$ is close to the experimental result. It is considered that this value of θ is reasonable for the combination of R-113 and sapphire.

Summarizing the results mentioned above, it can be concluded that the contact-line-length density is one of the very important quantities representing directly boiling heat transfer.

3. Observation of cross-sectional structure of boiling

As mentioned in the previous section, the liquid network coexisting with closely packed dry areas was observed at heat fluxes near CHF and this situation is very different from the three-layered boiling-structure model. In this section, a quasi-two-dimensional boiling system is proposed to observed the sectional views of the boiling structures and some experimental results are summarized.

3.1. Quasi-two-dimensional boiling system

A schematic diagram of the experimental apparatus used in this experiment is shown in Fig. 10(a). The test liquid was ethanol at atmospheric pressure and it was stored in a glass vessel of 110 mm in width, 25 mm in depth, and 80 mm in height. The test liquid was held at the saturation temperature by an electric heater which was set aside from the test section.

A schematic diagram of the boiling surface is shown in Fig. 10(b). The boiling surface was a horizontal plate

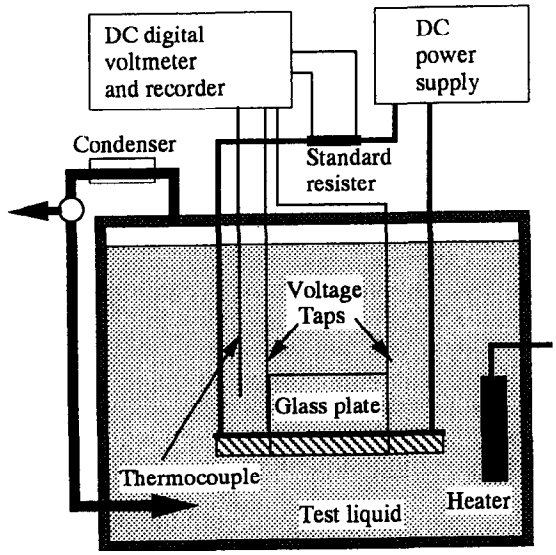

(a) Experimental apparatus

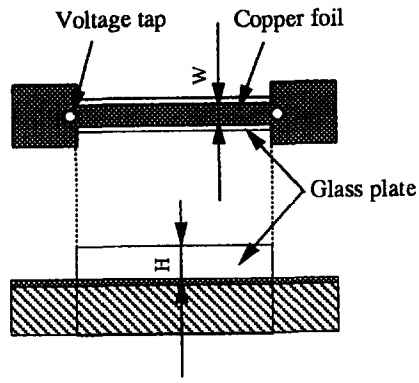

(b) Heat transfer surface

Fig. 10. Schematic diagram of experimental apparatus to observe bubble structures in quasi-two-dimensional space.

of epoxy resin with a copper film of 30 μm thickness on one side. The total thickness of the plate was 1.6 mm. The length of the test section of the copper film was 40 mm which was larger than the most dangerous wavelength of Rayleigh–Taylor instability for ethanol (17 mm). As shown in Fig. 10(b), the horizontal boiling surface was sandwiched by two vertical glass plates to realize a quasi-two-dimensional boiling space. The width of the boiling surface or the gap between the vertical glass plates was much smaller than the most dangerous wavelength ($W = 0.5$, 1.0, and 2.0 mm). The height of the glass plates was changed from $H = 0$ to 15 mm.

Boiling of the test liquid was activated by flowing a DC current in the copper film. A block of epoxy resin of 9 mm in thickness was attached to the back of the boiling

surface to reduce heat loss through the epoxy resin plate. To calculate the temperature of the copper film from its electric resistance, the DC current flowing in the film and the voltage between the voltage taps shown in Fig. 10(b) were measured. The measurement was repeated by increasing the electric current step by step, and it was continued until burnout of the copper film occurred. The calibration of the electric resistance to temperature was conducted for each boiling surface. The surface of the copper film was polished by emery papers of #3000 to make uniform the experimental condition.

The boiling structures between the glass plates were observed through the glass plate by using the high-speed video system (500 and 1000 frames/s).

3.2. Nucleate boiling curve and CHF in quasi-two-dimensional space

Figure 11 shows experimental data of the nucleate boiling curve together with that predicted from the correlation of Nishikawa and Fujita [18] and the value of CHF predicted from the theoretical model by Zuber [19]. As seen from the figure, no remarkable effect of W on the nucleate boiling curve is found.

In Fig. 12, the experimental data of CHF normalized by the Zuber equation, $q_{CHF}/q_{CHF,Z}$, are plotted to the surface width normalized by the Laplace length, W/λ_{cp}. In the figure, experimental data for $H = 0$ mm reported by Shoji and Kuroki [14] are also plotted. It is found from the figure that, in the case of $H = 0$ mm, the normalized CHF starts to increase if the normalized width is decreased below about two. It is found further that the normalized CHF is about unity regardless of the width if H is larger than 2 mm.

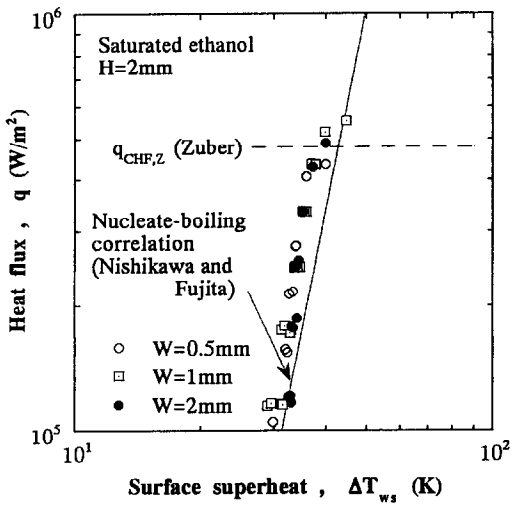

Fig. 11. Nucleate boiling curves in quasi-two-dimensional space ($H = 2$ mm).

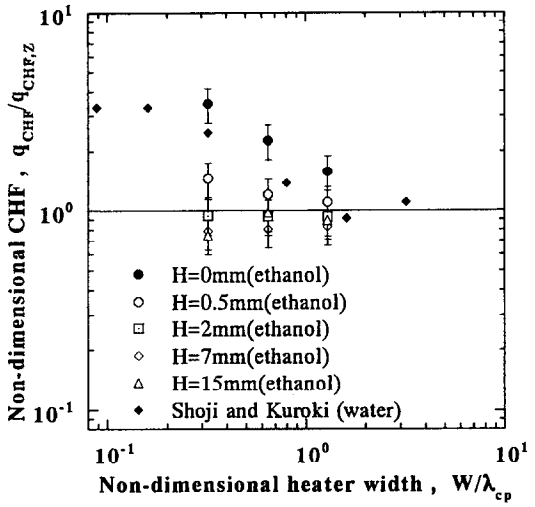

Fig. 12. Critical heat flux in quasi-two-dimensional space.

Summarizing the results mentioned above, boiling heat transfer in the quasi-two-dimensional space used in this experiment is not much different from that in usual three-dimensional spaces.

3.3. Bubble structures

Figure 13 shows typical video pictures obtained in this observation at three heat-flux levels for $W = 0.5$ mm and $H = 2$ mm. The left-side pictures at each heat-flux level are two successive close-up pictures taken at 1000 frames/s. The right-side picture is a distant-view picture taken at 500 frames/s to give a whole image of nucleate boiling.

In the case of Fig. 13(a) at $q = 0.15q_{CHF}$, bubbles are isolated with each other as shown in the right-side picture, but, as shown in the left-side pictures, the bubble departure is delayed due to the vertical coalescence of the departure bubble with a small bubble growing beneath the departure bubble.

The left-side pictures of Fig. 13(b) at $q = 0.3q_{CHF}$ indicate the initiation of the lateral coalescence of neighboring primary bubbles. As a result, as shown in the right-side picture, bubbles of large vapor mass are produced.

In the case of Fig. 13(c) at $q = 0.92q_{CHF}$, bubbles of very large mass, which can be called the filmwise bubbles, are formed. Figure 14 shows a set of successive pictures obtained at $q = 0.92q_{CHF}$. A filmwise bubble like a vapor film is observed in Fig. 14(a), and wavy motion is observed on its upper interface. In this case, the height of vertical glass plates is H = 2 mm and the convex parts of the wave protrude from the quasi-two-dimensional space. So, the convex parts are round off and recorded black. As shown with the arrow in Fig. 14(b), the filmwise bubble collapses at valleys of the wave and bubble gen-

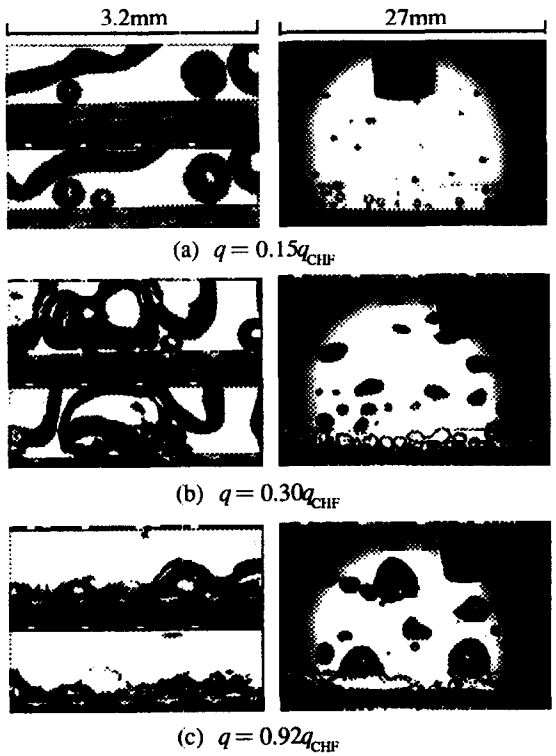

Fig. 13. Dependence of bubble structure on heat flux ($W = 0.5$ mm, $H = 2$ mm).

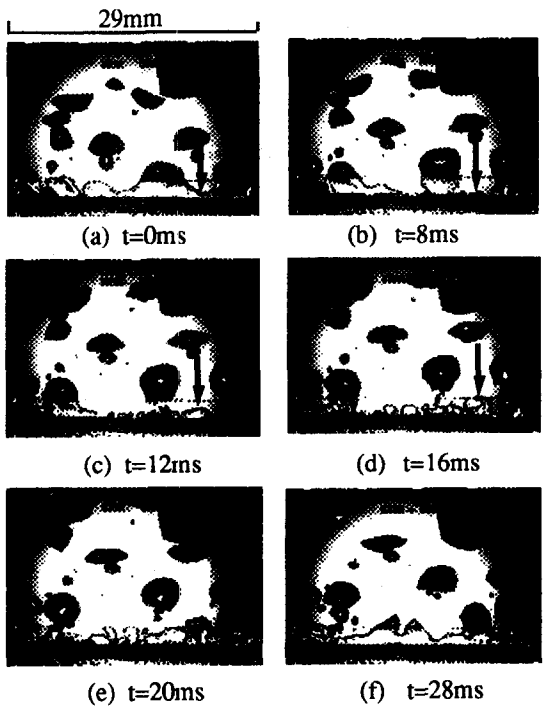

Fig. 14. Dynamic behavior of filmwise bubble ($W = 0.5$ mm, $H = 2$ mm, $q = 0.92q_{CHF}$).

eration occurs there. These bubbles coalesce each other and form secondary bubbles. The secondary bubbles coalesce repeatedly and a filmwise bubble is established again as shown in Fig. 14(f). This result indicates that the filmwise bubble is formed by lateral coalescence of bubbles. The left-side pictures in Fig. 13(c) show the structure under the filmwise bubble. The bubble structure at this heat flux level is more clearly shown in Fig. 15. It is clearly seen that a liquid film does exist between the surface and the filmwise bubble and also vigorous bubble generation does occur in the liquid film. This result gives an image of the boiling structure different from the three-layered model, but it is similar to the results obtained by Galloway and Mudawar [20] for forced convection boiling in a narrow channel. In this paper, following their paper, the liquid film including bubble generation is called the liquid subfilm.

It is considered that the physical situation named as the liquid–solid contact of the network pattern results from the formation of the liquid subfilm. The microlayer under the primary bubbles growing in the liquid subfilm seems to easily dryout because such bubbles grow like vapor domes and they would not easily depart from the surface. In this situation, wetted areas exist only between such bubbles like domes and then network-like canals are formed. More detailed observation will be necessary to confirm the relation between liquid canals and liquid subfilms because the width of liquid subfilm between the vapor domes shown in Fig. 15 seems larger than the width of liquid canals in Fig. 2(e).

In the existing CHF models (for example, Haramura and Katto [3]), the lateral pitch of departure of coalescent bubbles has been assumed equal to the most dangerous wavelength of Rayleigh–Taylor instability. In the present experiment using the quasi-two-dimensional space, we can clearly observe the departure process of coalescent bubbles. As already shown, the upper interface of the filmwise bubble is wavy and the bubble departure occurs at the convex part of the wave. Figure 16 shows the experimental data of the lateral pitch of the bubbles departing from the filmwise bubble. The experimental data are located near the most dangerous wavelength. These results indicate that bubble departure from the filmwise bubbles is controlled by the Rayleigh–Taylor instability at the upper interface of the filmwise bubbles.

In the CHF model proposed by Haramura and Katto

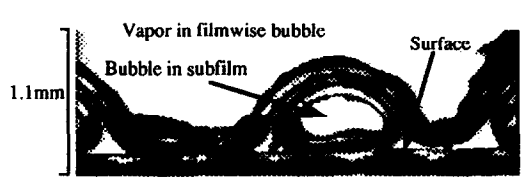

Fig. 15. Close-up picture of liquid film under filmwise bubble ($W = 0.5$ mm, $H = 2$ mm, $q = 0.92q_{CHF}$).

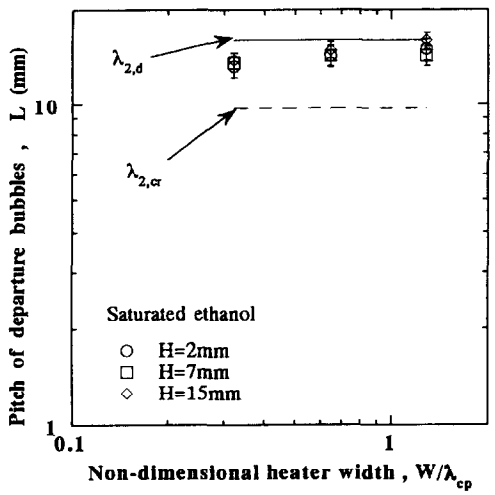

Fig. 16. Pitch of departure bubbles.

[3] based on the three-layered boiling-structure model, macrolayer thickness is one of the most important quantities which determine the critical heat flux. So, the liquid subfilm thickness under coalescent bubbles is discussed here. Figure 17 shows experimental results of the liquid subfilm thickness measured from magnified video pictures. The data shown by open symbols, $\delta_{l,min}$, are the thickness of liquid subfilm surrounding vapor domes and the data shown by solid symbols, $\delta_{l,max}$, are the height of vapor domes. The values of $\delta_{l,min}$ and $\delta_{l,max}$ vary with time. In the present study, they were determined by averaging the instantaneous values in each picture for a period much longer than the departure period of coalescent bubbles. In Fig. 17, the experimental results of 'macrolayer' thickness by Rajvanshi et al. [21] and the calculation

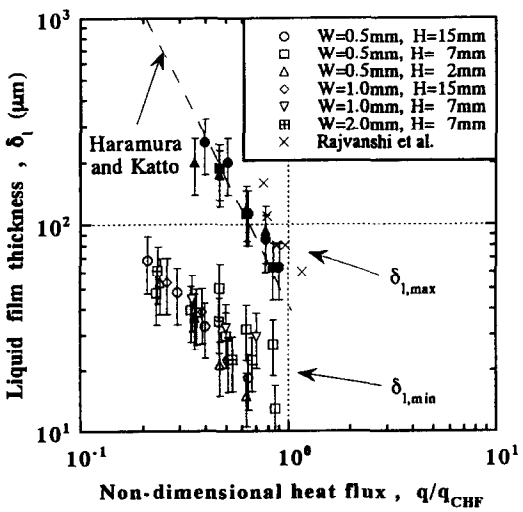

Fig. 17. Liquid subfilm thickness under coalescent bubbles.

results of 'macrolayer' thickness in Haramura and Katto model are also plotted. The results of $\delta_{l,max}$ show almost the same tendency with the existing results of 'macrolayer' thickness, but those of $\delta_{l,min}$ are much smaller than the 'macrolayer' thickness.

4. Conclusion

In the present paper, boiling structures such as liquid–solid contact patterns and bubble structures near the boiling surface were investigated experimentally by observing both the dynamic behavior of liquid–solid contact from below the surface and the sectional views of bubbles in a quasi-two-dimensional boiling space. The results are summarized as follows.

(1) As the surface superheat increases, the dry areas vary from the primary dry area to the secondary and tertiary dry areas and the liquid–solid contact pattern changes from the continuous plane pattern to the network and isolated patterns.

(2) The distribution of equivalent diameter of dry areas consists of the small and large diameter regions. In the small diameter region, the number density of dry areas is independent of the diameter, but in the large diameter region it rapidly decreases with increase in diameter.

(3) The liquid–solid contact structure in high heat-flux boiling is the liquid network coexisting with closely packed dry-areas and the bubble structure is the combination of primary bubbles generated in a thin liquid film with filmwise bubbles covering the primary bubbles. Bubble departure from the filmwise bubbles occurs by the Rayleigh–Taylor instability.

(4) The contact-line-length density was proposed as a new measure of the contribution of liquid–solid contact to high heat-flux boiling heat transfer. The dependence of the contact-line-length density on surface superheat is very similar to the boiling curve.

References

[1] Asai A. Application of the nucleation theory to the design of bubble jet printers. Japanese Journal of Applied Physics 1989;28:909–15.

[2] Gaertner RF. Photographic study of nucleate pool boiling on a horizontal surface. Transactions of the ASME, Journal of Heat Transfer 1965;87;17–29.

[3] Haramura Y, Katto Y. A new hydrodynamic model of critical heat flux, applicable widely to both pool and forced convection boiling on submerged bodies in saturated liquids. International Journal of Heat and Mass Transfer 1983;26:389–99.

[4] Dhir VK, Liaw P. Framework for a unified model for

nucleate and transition pool boiling. Transactions of the ASME, Journal of Heat Transfer 1989;111:739–46.

[5] Katto Y, Yokoya S. Principle mechanism of boiling crisis in pool boiling. International Journal of Heat and Mass Transfer 1968;11:993–1002.

[6] Nagai N, Nishio S. A method for measuring the fundamental quantities on liquid–solid contact in pool boiling using an image processing technique. Flow Visualization and Image Processing of Multiple Systems, FED-V.209, ASME, 1995. pp. 73–9.

[7] Oka T, Abe Y, Mori YH, Nagashima A. Pool boiling of *n*-pentane, CFC-113, and water under reduced gravity: parabolic flight experiments with a transparent heater. Transactions of the ASME, Journal of Heat Transfer 1995;117:406–17.

[8] Nishio S. Cooldown of insulated metal plates. Proceedings of 1983 ASME/JSME Thermal Engineering Joint Conference, Vol. 1. Hawaii, 1983. pp.103–9.

[9] Nagai N, Nishio S. Leidenfrost temperature on an extremely smooth surface. Experimental Thermal and Fluid Science 1996;12:373–9.

[10] Ragheb HS, Cheng SC. Surface wetted area during transition boiling in forced convective flow. Transactions of the ASME, Journal of Heat Transfer 1979;101:381–3.

[11] Lee LYW, Chen JC, Nelson RA. Liquid–solid contact measurements using a surface thermocouple temperature probe in atmospheric pool boiling water. International Journal of Heat and Mass Transfer 1985;28:1415–23.

[12] Dhuga DS, Winterton RHS. Measurement of surface contact in transition boiling. International Journal of Heat and Mass Transfer 1985;28:1869–80.

[13] Neti S, Butrie T, Chen JC. Fiber-optic liquid contact measurements in pool boiling. Rev Sci Instrum 1986;57:3043–47.

[14] Shoji M, Kuroki H. Non-linear aspects of high heat flux nucleate boiling heat transfer-formulation and results. Proceedings of 1994 IMECE. HTD-V.298, ASME, 1994. pp. 91–114.

[15] Tanasawa I. Advances in condensation heat transfer. Advances in Heat Transfer. Academic Press, 1991;21:55–139.

[16] Carey Van P. Liquid–vapor phase-change phenomena. Orlando: Academic Press. New York: Hemisphere, 1992. Chapters 2 and 7.

[17] Graham RW, Hendricks RC. Assessment of convection, conduction and evaporation in nucleate boiling. NASA Technical Note, 1967, TN D-3943. pp. 1–42.

[18] Nishikawa K, Fujita Y. Nucleate boiling heat transfer and its augmentation. Advances in Heat Transfer 1990;20: 1–82. Orlando: Academic Press.

[19] Zuber N, Tribus M, Westwater JW. The hydrodynamic crisis of pool boiling of saturated and subcooled liquids. Unt Dev in Heat Transfer. New York: ASME, 1963. pp. 230–235.

[20] Galloway JE, Mudawar I. CHF mechanism in flow boiling from a short heated wall—I. Examination of new-wall conditions with the aid of photomicrography and high-speed video imaging. International Journal of Heat and Mass Transfer 1993;30:2511–26.

[21] Rajvanshi AK, Saini JS, Prakash R. Investigation of macrolayer thickness in nucleate pool boiling at high heat flux. International Journal of Heat and Mass Transfer 1992;35:343–50.